Computer Methods and Programs in Biomedicine 142 (2017) 21–30

Contents lists available at ScienceDirect

Computer Methods and Programs in Biomedicine

journal homepage: www.elsevier.com/locate/cmpb

A numerical model for aggregations formation and magnetic driving of spherical particles based on OpenFOAM®

E.G. Karvelas [a,*], N.K. Lampropoulos [b], I.E. Sarris [b]

[a] Department of Civil Engineering, University of Thessaly, Pedion Areos, 38221 Volos, Greece
[b] Department of Energy Technology, Technological & Educational Institute of Athens, Ag. Spyridona 17, 12210 Athens, Greece

ARTICLE INFO

Article history:
Received 12 May 2016
Revised 28 January 2017
Accepted 9 February 2017

Keywords:
Aggregations
Magnetic driving
CFD
Cancer therapy

ABSTRACT

Background and objective: This work presents a numerical model for the formation of particle aggregations under the influence of a permanent constant magnetic field and their driving process under a gradient magnetic field, suitably created by a Magnetic Resonance Imaging (MRI) device.
Methods: The model is developed in the OpenFOAM platform and it is successfully compared to the existing experimental and numerical results in terms of aggregates size and their motion in water solutions. Furthermore, several series of simulations are performed for two common types of particles of different diameter in order to verify their aggregation and flow behaviour, under various constant and gradient magnetic fields in the usual MRI working range. Moreover, the numerical model is used to measure the mean length of aggregations, the total time needed to form and their mean velocity under different permanent and gradient magnetic fields.
Results: The present model is found to predict successfully the size, velocity and distribution of aggregates. In addition, our simulations showed that the mean length of aggregations is proportional to the permanent magnetic field magnitude and particle diameter according to the relation : $\tilde{l}_a = 7.5 B_0\, d_i^{3/2}$. The mean velocity of the aggregations is proportional to the magnetic gradient, according to : $\tilde{u}_a = 6.63 \tilde{G} B_0$ and seems to reach a steady condition after a certain period of time. The mean time needed for particles to aggregate is proportional to permanent magnetic field magnitude, scaled by the relationship : $\tilde{t}_a \propto 7 B_0$.
Conclusions: A numerical model to predict the motion of magnetic particles for medical application is developed. This model is found suitable to predict the formation of aggregations and their motion under the influence of permanent and gradient magnetic fields, respectively, that are produced by an MRI device. The magnitude of the external constant magnetic field is the most important parameter for the aggregations formation and their driving.

1. Introduction

Chemotherapy is used for the fight against cancer cells and tumors, where drug is injected into the body from arteries and results in general systemic distribution that may result in toxic side-effects as the drug attacks both healthy and cancer cells [1]. Researchers in the late 70s have proposed navigation of drug-loaded magnetic particles towards the tumors by using external magnetic fields [2,3] in order to reduce the side-effects of chemotherapy. Since the healthy tissue is spared, the side-effects of this method are minimized, while at the same time the therapeutic efficiency is enhanced through the increased quantity of drug that may reach the area of interest in the human body. For the navigation of iron-core particles to the targeted area, high gradient magnetic fields should be applied and devices such as Magnetic Resonance Imaging (MRI) may be used.

The efficiency of the magnetic guided drug delivery method depends on blood flow rates, pore size and several other physical parameters, as commented out in Ref. [4–6]. In a first place, the materials, from which the magnetic particle cores and their coatings are constructed, are important due to the variety of magnetic properties (i.e. magnetic permeability, see for example [7]). The size of particles is also critical for the effectiveness of the proposed method. It is found that the smaller the particles size is, the weaker their magnetic response will be, resulting in increased difficulty for particles to be driven into artery bifurcations. Pankhurst et al. [4] suggest that imperative magnets should be used for the particles' navigation. Moreover, in order to overcome this difficulty, magnetic particles form clusters of 'magnets' under the influence of permanent magnetic fields by attracting each other if close enough (example Ref. [8]). These clusters of

* Corresponding author.
E-mail address: Karvelas@civ.uth.gr (E.G. Karvelas).

http://dx.doi.org/10.1016/j.cmpb.2017.02.017
0169-2607/

Nomenclature

u	Fluid velocity
p	Pressure
ρ	Density
μ	Viscocity
m	Mass
d_i	Diameter
$\boldsymbol{u}$	Transversal velocity
$\boldsymbol{\omega}$	Rotational velocity
t	Time
$\boldsymbol{I}$	Mass moment of inertia matrix
$\boldsymbol{F}_{mag}$	Total magnetic force
$\boldsymbol{F}_{nc}$	Normal contact force
$\boldsymbol{F}_{tc}$	Tangential contact force
$\boldsymbol{F}_{drag}$	Hydrodynamic drag force
$\boldsymbol{F}_{grav}$	Gravity and buoyancy force
$\boldsymbol{M}_{drag}$	Drag moment
$\boldsymbol{M}_{con}$	Contact moment
$\boldsymbol{T}_{mag}$	Torque due to magnetic field
$\boldsymbol{F}_{intmag}$	Magnetic force due to the interaction of particles with the magnetic field
$\boldsymbol{F}_{ismag}$	Magnetic force due to the interaction of particles
μ_0	Magnetic permeability of free space
μ_r	Relative magnetic permeability of the particle
$\hat{\boldsymbol{r}}$	Distance between particles
V	Volume of the spherical particle
$\boldsymbol{m}$	Magnetic moment of particle
$\boldsymbol{B}$	Magnetic field in the MRI bore
$\boldsymbol{B_0}$	Constant field
$\tilde{\boldsymbol{G}}$	Gradient field
$\boldsymbol{B}_1$	Time dependent radio frequency field
$\bar{l}_a$	Mean length of aggregations
$\bar{t}_a$	Total time
$\bar{u}_a$	Mean velocity of aggregates

Subscripts

mag	Magnetic
nc	Natural contact
tc	Tangential contact
grav	Gravity
con	Contact
intmag	Interaction with magnetic field
ismag	Interaction with surrounding magnetic particles
r	Relative

particles form chains that are line up to the external magnetic field and are more sensitive to gradient magnetic fields than single particles, since their total magnetic moment is higher [9]. Once the aggregations are navigated close to the target area, they can break up into isolated particles by switching off the magnetic field in order to facilitate the drug release [8]. In the case of magnetic nanoparticles, the weak magnetic moment of single particles can also be increased when many particles are attached on carbon nanotubes (see for example [10]). The advantages of magnetic nanoclusters include tunable cluster size, efficient drug loading and enhanced particle uptake in cancer cells with no apparent decrease in the inherent magnetization characteristics [11]. In addition, the drug loaded nanoclusters under the influence of the magnetic field can reduce hemodynamics of stenosis [12,13].

The strength of the applied permanent magnetic field is also important since weak magnetic fields can only create small aggregations due to weak dipole interaction forces that may be act only between a few particles [14]. In addition, navigation of small aggregations from gradient magnetic fields is not possible because of their weak total magnetic moment. On the other hand, aggregations of large size could form clots in small arteries, especially when aggregates pass through possible stenosis in these arteries. The ratio of aggregates velocity to the velocity of an individual particle is found to reach a constant value independent of the size aspect ratio between a single particle and the aggregate [15]. As van Netten et al. [16] report, the magnetization of particles increases as a result of the increase of concentration of matter along the direction of the field, and this increase leads to a moderate change in velocity. Finally, Gleich et al. [17] found that the magnetic force decreases as the distance from the electromagnetic coil increases. In order to overcome this difficulty, magnets should be implemented near the targeted sites [18–20].

In the present work, a numerical model for the formation of particle aggregations and their magnetic driving based on OpenFOAM® platform is proposed. The major features of the model are: (i) the simulation of the particle aggregation process under the action of permanent external magnetic fields, (ii) the interaction of particles under the combined action of different forces, and (iii) their motion in a fluid environment under the driving force of gradient magnetic fields. The governing equations and all important numerical details are presented in Section 2. The validation of the model against existing experimental and numerical results, as well as, numerical simulations with different parameters are presented in Section 3. Results from several parametric studies to estimate the mean aggregation length, velocity and time under various permanent and gradient magnetic fields are discussed in Section 4 for two kinds of particles. Finally, conclusions are presented in Sections 5.

2. Numerical model

The general purpose numerical library OpenFoam [21] is used in two and three dimensional domains as a frame for the simulation of fluid and particles flow in suspensions. As the fluid flow is expected to be laminar and steady-state, the incompressible Navier–Stokes equations were solved for the Eulerian phase together with a Lagrangian model for the tracking of particles in the discrete phase. The laminar governing equations of the fluid phase are given by [22]:

$$\nabla \cdot u = 0 \tag{1}$$

$$\rho\left(\frac{\partial u}{\partial t} + u \cdot \nabla u\right) = -\nabla p + \mu \nabla^2 u \tag{2}$$

where, u and p are the fluid velocity and pressure, respectively, and ρ and μ are its density and viscosity, respectively.

No coupling between the fluid and the discrete phases is considered for the small number of particles that is considered here. Since the Eulerian phase is known to work well in OpenFoam, both in hydrodynamic and magnetohydrodynamic flows [23], our attention is focused on the magnetic particles discrete model. Thus, for testing this model, only simulations with fluids at rest where conducted, in order to mimic existing relevant experimental and numerical results from the particle drug delivery literature as described below.

The discrete model includes all the important forces that may be applied on particles. Briefly the forces are: (a) the magnetic force that is exerted from the permanent magnet of the MRI, and leads the particles to behave like dipoles and attract each other. This attraction force is responsible for the formation of the aggregations. (b) The magnetic gradient force that is exerted from the special propulsion gradient coils of the MRI and is able to navigate the particles and the aggregations. Details of the numerical model for the magnetic forces can be found in [24]. (c) The contact

force between the particles and the walls is calculated by using the discrete element method (DEM), which includes spring and damping models [25]. (d) The drag force is calculated on conglomerates through a novel approach to determine the drag coefficient, C_d, a model where only the surface of the particles in the aggregations is directly exposed to the fluid is taken into account in the calculation of drag force [26]. (e) Gravity and buoyancy forces are added to the numerical model. Although, these forces are negligible for isolated particles, when particles are formed into aggregates may play a significant role. Numerical details of the model for the contact, fluid, gravity and buoyancy forces are given by Lampropoulos et al. [26]. It should be noted that the Van der Waals force is not accounted in the model since it is acting in a relatively small range and can be masked by interactions of longer range, such as magnetic dipole - dipole interactions [27]. Finally, Brownian forces are not taken into account since at the micro scale, stochastic Brownian motion is negligible compared to the particle size [28].

The equations of every particle single motion in the discrete model are given by Oda and Iwashita [29] and are based on the Newton law and may read as:

$$m_i \frac{\partial \boldsymbol{u}_i}{\partial t} = \boldsymbol{F}_{mag,i} + \boldsymbol{F}_{nc,i} + \boldsymbol{F}_{tc,i} + \boldsymbol{F}_{drag,i} + \boldsymbol{F}_{grav,i} \tag{3}$$

$$\boldsymbol{I}_i \frac{\partial \omega_i}{\partial t} = \boldsymbol{M}_{drag,i} + \boldsymbol{M}_{con,i} + \boldsymbol{T}_{mag,i} \tag{4}$$

where, the index i stands for the ith-particle with diameter d_i, $\boldsymbol{u}_i$ and $\boldsymbol{\omega}_i$ are its transversal and rotational velocities, respectively and m_i is its mass. The quantity t stands for the time, the mass moment of inertia matrix is $\boldsymbol{I}_i$, and the terms $\frac{\partial \boldsymbol{u}_i}{\partial t}$ and $\frac{\partial \omega_i}{\partial t}$ correspond to the linear and angular accelerations, respectively. $\boldsymbol{F}_{mag,\,i}$ is the total magnetic force, and $\boldsymbol{F}_{nc,\,i}$ and $\boldsymbol{F}_{tc,\,i}$ are the normal and tangential contact forces, respectively. $\boldsymbol{F}_{drag,\,i}$ stands for the hydrodynamic drag force. $\boldsymbol{F}_{grav,\,i}$ is the total force due to buoyancy. $\boldsymbol{M}_{drag,\,i}$ and $\boldsymbol{M}_{con,\,i}$ are the drag and the contact moments, respectively. Finally, $\boldsymbol{T}_{mag,\,i}$ is the torque due to the magnetic field at the position of particle i. All forces and moments are calculated according to DEM method as in [25] and the magnetic force is given by the total applied field [30–32], $\boldsymbol{F}_{mag,i} = \boldsymbol{F}_{intmag,i} + \boldsymbol{F}_{ismag,i}$, where, the magnetic force due to the interaction of the ith particle with the magnetic field produced in the MRI bore, $\boldsymbol{B}$, is given by $\boldsymbol{F}_{intmag,i} = V(\boldsymbol{m}_i \cdot \nabla)\boldsymbol{B}$, where, V is the volume of the spherical particle. The magnetic force is acting on the ith particle due to its interaction with the surrounding magnetic particles is given by $\boldsymbol{F}_{ismag,i} = \sum_j^N \boldsymbol{F}_{ismag,ji}$, where, the magnetic force exerted in particle i due to particle j can be found by [32]:

$$\begin{aligned}\boldsymbol{F}_{ismag,ji} = \frac{3\mu_0 m_i m_j}{4\pi r_{ji}^4}[&\hat{\boldsymbol{r}}_{ji}(\hat{\boldsymbol{m}}_i \cdot \hat{\boldsymbol{m}}_j) + \hat{\boldsymbol{m}}_i(\hat{\boldsymbol{r}}_{ji} \cdot \hat{\boldsymbol{m}}_j) \\ &+ \hat{\boldsymbol{m}}_j(\hat{\boldsymbol{r}}_{ji} \cdot \hat{\boldsymbol{m}}_i) - 5\hat{\boldsymbol{r}}_{ji}(\hat{\boldsymbol{r}}_{ji} \cdot \hat{\boldsymbol{m}}_i)(\hat{\boldsymbol{r}}_{ji} \cdot \hat{\boldsymbol{m}}_j)]\end{aligned} \tag{5}$$

where, μ_0 is the permeability of free space, $\hat{\boldsymbol{r}}_{ji}$ is the distance between i and j particles.

The magnetic moment, $\boldsymbol{m}_i$, of the ith particle is given by $\boldsymbol{m}_i = \frac{4\pi}{\mu_0}\frac{\mu_r - 1}{\mu_r + 2}\frac{d_i^3}{8}\boldsymbol{B}_i$ [32], the magnetic field acting on the ith particle can be found by $\boldsymbol{B}_i = \boldsymbol{B} + \sum_j^N \boldsymbol{B}_{ji}$, and $\boldsymbol{B}_{ji} = \frac{\mu_0}{4\pi}[\frac{3(\boldsymbol{m}_j \cdot \boldsymbol{r}_{ji})\boldsymbol{r}_{ij}}{\boldsymbol{r}_{ji}^5} - \frac{\boldsymbol{m}_j}{\boldsymbol{r}_{ji}^3}]$, where, μ_r is the magnetic permeability of the particle.

The OpenFOAM® platform [21] is used for the calculation of fluid flow field and the motion of particles. In a first place, the calculation of the flow field is achieved by coupling the velocity with pressure by using the pressure implicit with splitting of operators (PISO) method. After the determination of the flow and pressure fields, the Lagrangian motion of particles is evaluated by solving Eqs. (3) and (4) along the trajectory of each particle. The implicit Euler method is used for time marching the equations and the time step is set to 10^{-6} s in order to ensure the stability of the algorithm.

2.1. Magnetic field and interaction domain

The magnetic field $\boldsymbol{B}$ in the MRI bore is given by

$$\boldsymbol{B} = \boldsymbol{B}_0 + \tilde{\boldsymbol{G}} + \boldsymbol{B}_1 \tag{6}$$

where, $\boldsymbol{B}_0$ is the MRI superconducting magnetic field that is considered constant and uniform, $\tilde{\boldsymbol{G}}$ is the gradient field and $\boldsymbol{B}_1$ is the time dependent radio frequency field [33], that is considered zero in the present work.

It is obvious from Eq. (5) that the magnetic interaction force ($\boldsymbol{F}_{mag}$), in the parallel direction between two spheres, is inversely proportional to the fourth power of the separation distance [34,35]:

$$\boldsymbol{F}_{mag} \propto \frac{m_i m_j}{r_{ji}^4} \tag{7}$$

From Eq. (7) is evident that a weak interaction is observed between a pair of particles that are located away from each other. However, the velocity of the approaching particles is getting higher due to the increasing magnetic force.

It is known that the stronger the magnetic field is, the magnetic moment of the particles will be bigger. As a result, each particle affect the other within an area that is called interaction distance. As Lampropoulos et al. [36] found, the interaction distance depends primarily on the external magnetic field, and secondary on the size and material of the particles. In order to reduce the computational time, preliminary simulations to measure the maximum interaction distance of each particle were conducted and found that the interaction distance is $15d_i$ for $\boldsymbol{B}_0$ up to $0.5T$, $25d_i$ for $0.5T < \boldsymbol{B}_0 < 0.8T$ and $32d_i$ for $\boldsymbol{B}_0 > 0.8T$. Interactions among particles that are located only inside this distance range, are taken into account by the present algorithm for the calculation of the magnetic moment of particles. Particles that are located outside this distance automatically are rejected by the algorithm. The speed of the algorithm is further improved by packing the magnetic moments of all particles within each cloud defined by interacting particles. In this way, magnetic moments are automatically recalled in order to be used for the calculation of other particles. Simulations of 64 and 125 particles of the above mentioned method show agreement in half time in contrast to the method of calculating the magnetic moments exerted on particle from all other particles for every time step.

3. Results

The present numerical model is validated against the results from Refs. [8,24]. In order to perform the comparisons, two series of simulations with the following computational domains and grid distributions are selected:

(a) In the first case, four water solutions with different concentrations are simulated under the magnetization of a uniform magnetic field in a stationary fluid. The spacing of the three-dimensional computational grid is kept equal to $2d_i$ in each direction.

(b) In the second case, a distilled stationary water solution with concentration of 25 mg/ml consisted of 88 polystyrene magnetic particles with 5.5 μm diameter is simulated under a constant magnetic field of $B_0 = 0.005T$ and a gradient magnetic field of $\tilde{G} = 1.4$ T/m along the $x-$axis. The spacing of the two-dimensional domain is kept $5d_i$ in each direction. The summary of the domain parameters for the first and second cases is shown in Table 1.

In the first test case, the density of the Fe_3O_4 particles and the fluidic environment is 1087 kg/m^3 and 1000 kg/m^3, respectively,

Table 1
Simulation parameters.

Flow domain and computational details of Case 1 (3D)								
No	Concentr. (mg/ml)	Particle number	Volume (m^3)	Dimensions (m) $\times 10^4$ of $x \times y \times z$ directions			Number of cells (x,y,z)	Sim. time (cpu-h)
1	0.563	311	4.185×10^{-10}	7.48	7.48	7.48	$34 \times 34 \times 34$	24.48
2	1.125	385	2.596×10^{-10}	6.38	6.38	6.38	$29 \times 29 \times 29$	55.68
3	2.25	1003	3.38×10^{-10}	7.04	7.04	6.82	$32 \times 32 \times 31$	487.2
4	4.5	1497	5.174×10^{-11}	6.38	6.38	6.16	$29 \times 29 \times 28$	660.0
Flow domain and computational details of Case 2 (2D)								
5	25	88	4.159×10^{-13}	2.75	2.75	0.0275	10×10	1108.8

while the diameter of the particles is considered to be 11 μm as in Ref. [8]. The relative magnetic permeability of the Fe_3O_4 particles is 1.23 and the magnetic permeability of the fluid is 1.25×10^{-6} A/m. The Young's modulus of the material is 10^9 N/m^2, the tangential stiffness is 10 Nsm^{-1} and the coefficient of friction and the Poisson ratio have both the same value of 0.5.

Four water solutions with particle concentrations of 0.563, 1.125, 2.25 and 4.5 mg/ml with $300 - 1500$ particles are considered. No external magnetic gradient is applied during this simulation and the initial positions of the microparticles are randomly generated. At the beginning of each simulation, for $t \leq 0$, no magnetic field is applied, and for $t > 0$ a uniform transverse magnetic field of magnitude $B_0 = 0.4T$ is applied. Due to the influence of the permanent magnetic field, particles (magnetic dipoles) are formed into chains that are oriented parallel to the magnetic field direction. The agglomeration process is found to last for $t \simeq 5$ ms for all cases and particles are formed into chains as is showed in Fig. 1 and for the representative case of concentration 2.25 mg/ml.

Due to the external magnetic field, the magnetic particles are acting like magnets and the particle motion is attributed initially to gravity and magnetic interactions forces, since no fluid and particle flow exist. Then gradually drug force becomes important. The size of the aggregations formed as a function of particle number and concentration is presented in Table 2 for all four cases. Results for concentration 1.125 mg/ml show that four aggregates of a length of 10 particles may be formed due to the application of this magnetic field. It is observed that the size of the aggregations increases as concentration increases and chains of 73 particles may be found for 4.5 mg/ml. Results from the present model are compared against the experimental data of Ref. [8] as it is depicted in Fig. 2 and tabulated in Table 3 for the mean length and standard deviation of the aggregates size.

Fig. 2 shows the length of aggregates major axis whose average value follows an upward trend as a function of suspension concentration. The major axis length corresponds to the longest dimension of the aggregates measured. Larger aggregates are detected in increasing numbers as the concentration of the suspension increases. As it is observed, all mean aggregation lengths between the present numerical results and the experimental results of Ref. [8] are found to be very close. Small differences that may occur between these two cases are due to the small number of particles (up to 1500 particles) that are used in the present simulation in comparison to the experimental measurements that are conducted using a number of particles of the order of 10^6.

In the second case that is tested here, which is initially addressed by Vartholomeos and Mavroidis [24], the flow and aggregation of particles under the combined action of a constant and a gradient external magnetic field acting simultaneously is studied. The present results are compared against the experimental and numerical results of Ref. [24] for the motion of a magnetic suspension of polystyrene magnetic particles (5.5 μm) with density of 1050 kg/m^3 and concentration of 25 kg/m^3 in distilled water.

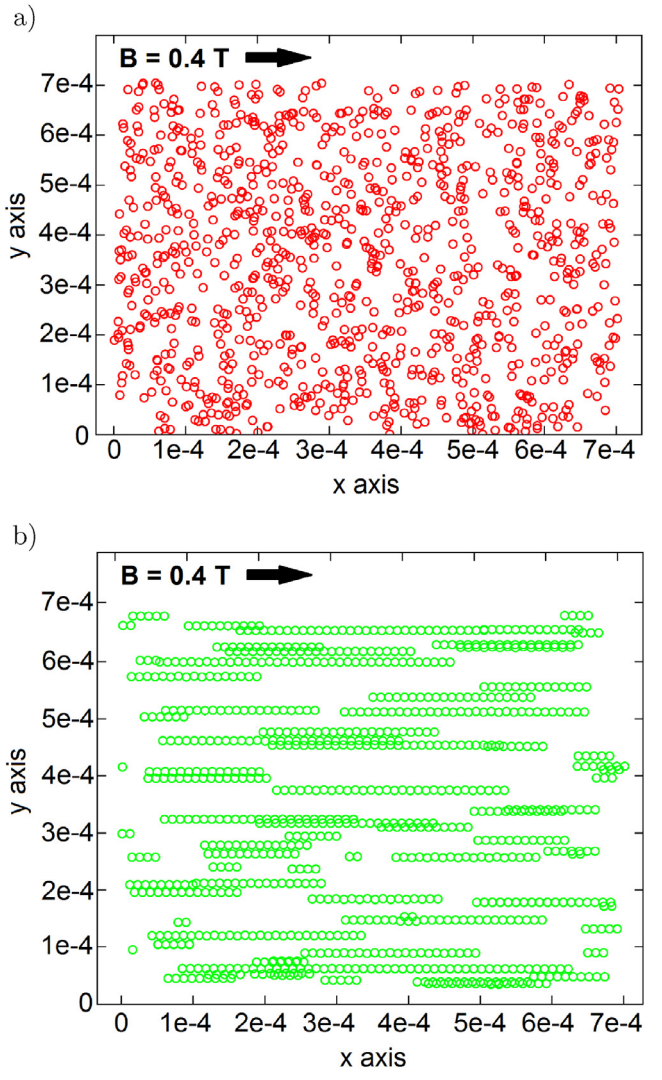

Fig. 1. Projection of particle positions at the (x-y)-plane. Red circles (a) dedicate the initial position of particles at $t = 0$ s for concentration 2.25 mg/ml, while green circles (b) correspond to the final positions of particles at $t \simeq 5$ ms, where the particles chains are fully oriented parallel to B_0. (For interpretation of the references to colour in this figure legend, the reader is referred to the web version of this article.)

Driven by the uniform magnetic field and the magnetic gradient along the $x-$axis, the microparticles are successively aggregated and simultaneously transported in the direction parallel to the magnetic gradient. Four instances at times 0.05 s, 0.1 s, 1 s and 4 s that show of the particle locations as they move are presented in Fig. 3. The mechanism of aggregates formation is found to de-

Table 2
Summary of the size of aggregations of Case 1.

	Particles per simulation			
Particles per aggregation	311 0.563 mg/ml	385 1.125 mg/ml	1003 2.25 mg/ml	1497 4.5 mg/ml
1	26	9	2	0
2	24	13	7	0
3	18	5	4	1
4	5	11	7	0
5	7	5	6	0
6	7	6	1	0
7	7	5	4	0
8	2	4	1	1
9	2	2	2	1
10	1	4	2	0
11	0	2	0	2
12	0	2	7	0
13	0	1	1	0
14	0	0	4	0
15	0	0	3	1
16	0	0	2	0
17	0	1	3	0
18	0	0	1	0
19	0	1	2	0
20	0	0	1	0
21	0	0	1	0
23	0	0	3	0
24	0	0	1	0
25	0	0	1	0
26	0	0	1	0
28	0	0	2	0
30	0	0	1	0
31	0	0	1	2
32	0	0	2	1
34	0	0	0	2
35	0	0	0	1
38	0	0	1	0
42	0	0	0	2
44	0	0	0	1
48	0	0	0	1
49	0	0	0	1
50	0	0	1	1
51	0	0	0	1
53	0	0	0	3
54	0	0	0	1
55	0	0	0	1
56	0	0	0	2
58	0	0	0	1
65	0	0	0	1
66	0	0	0	1
73	0	0	0	1

pend on their neighbour particles distance and magnetic momentum, based on that, particles may approach others or stay isolated. The duration for the formation of the aggregates in the present simulation is $t = 1.25$ s, while for larger times only translational motion of the aggregates is found. Thus, longer time is needed for the formation of aggregates in this case rather than in the first case studied, due to the smaller magnetic forces exerted by the weaker horizontal constant magnetic field.

Table 4
Comparison of present results from Case 2 against experimental and simulation results from Ref. [24].

Case	Mean size (particles)	std size (particles)	Mean velocity (μm/s)	std velocity (μm/s)
Experiment, Ref. [24]	7	5	7.5	1
Present	7.63	5.88	8.3	1.4
Numerical, Ref. [24]	10	4	9	2

The results of the present simulation are summarized and compared in Table 4 against the experimental data and numerical results of Ref. [24] in terms of mean values and standard deviations. It is observed that all results show good qualitative and quantitative agreement and moreover, results from the present model are closer to the experimental one than of the model proposed by Ref. [24]. Because, the present model is found to predict well the size, velocity and distribution of aggregates, it is used for further investigations of their formation and magnetic driving.

From the analysis above it is obvious that keeping the particle material fixed as in Ref. [24], the most important parameters for the formation and magnetic driving of aggregations are the permanent magnetic field magnitude B_0, the magnetic gradient $\tilde{G}$, and the diameter of particles d_i. Based on this observation, the effects of these three quantities are studied by using the present numerically model. The effect of B_0 is studied in the usual MRI working range by performing simulations for $0 \leq B_0 \leq 1T$ with increments of $0.1T$. The effect of $\tilde{G}$ is studied by progressively increasing its value from zero to 1 T/m, while the magnitude of B_0 is kept constant at 0.5 and $1T$. Furthermore, the above parametric study is performed for two kinds of spherical microparticles with $d_1 = 11$ μm and $d_2 = 22$ μm, as in Ref. [24,37] in order to balance between computational cost and usage of the present results. All simulations are conducted for 500 particles in a water solution of concentration 1.125 mg/ml by using the same physical properties as in the first test case of Ref. [8] for both fluid and particles.

4. Discussion

4.1. Effect of permanent magnetic field

Two series of simulations for particles with $d_1 = 11$ μm and $d_2 = 22$ μm are performed for each case by switching B_0 in the range $0.1T$ to $1T$ with increment of $0.1T$. It is known that, the increase of B_0 results in increasing the magnetic moment and interaction distance of particles [36]. As a result, more particles are interact each other and form bigger aggregates. These aggregations are formed by the presence of the permanent magnetic field [38] and aligned to the magnetic field lines [39,40]. Due to the action of higher B_0, particles interact each other with stronger magnetic force and at longer distances, and consequently are capable to form bigger chains parallel to the magnetic field lines, as tabulated in Table 5 and depicted in Fig. 4. The mean length of aggregations, $\bar{l}_a$, is the most suitable quantity to measure the size of particle chains. As shown in Fig. 4a, the increase of $\bar{l}_a$ for both kinds of particles is almost linear. However, for the same values

Table 3
Comparison of the present results against the experimental measurements from Ref. [8].

Concentr. (mg/ml)	Particle number	Mean length (μm) (simulation)	std (simulation)	Mean length (μm) (experiment)	std (experiment)
0.563	311	34.02	23.72	31	16
1.125	385	59.14	43.19	59	36
2.25	1003	140.36	110.45	137	85
4.5	1497	288.37	177.45	317	195

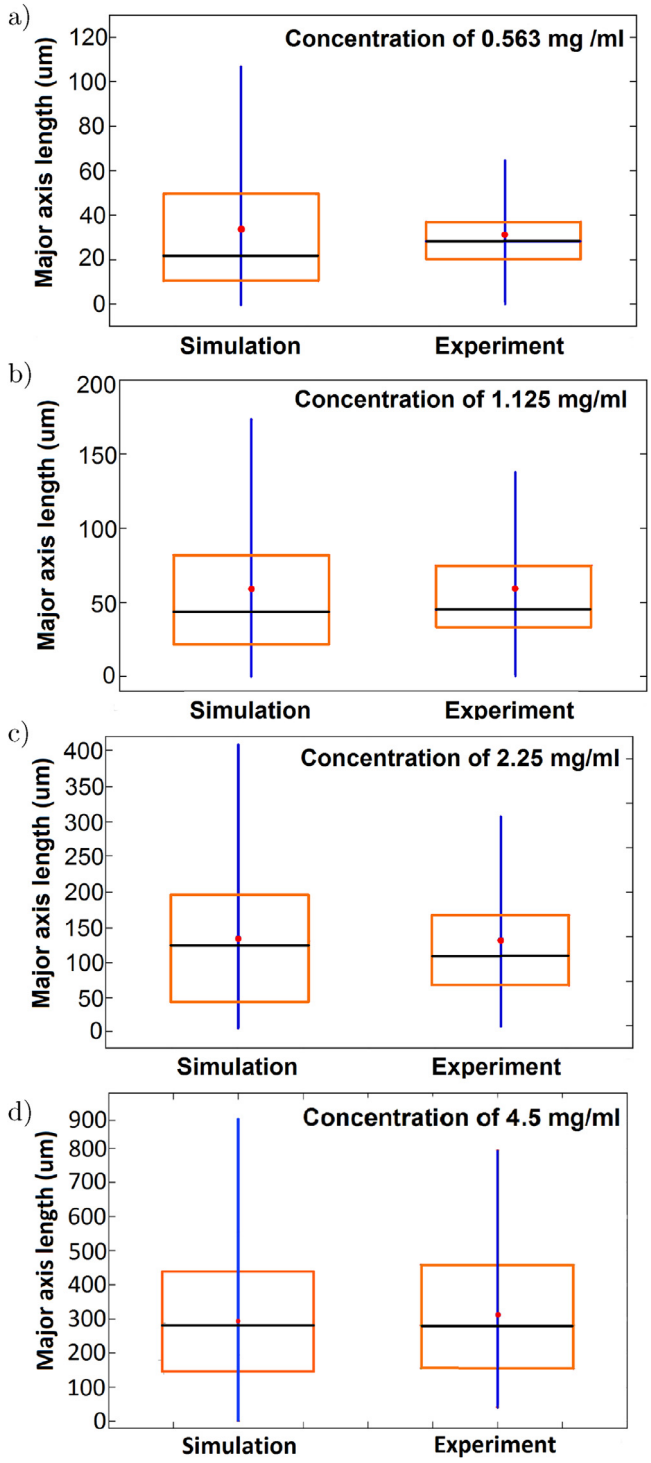

Fig. 2. Box plots show variations in the major axis length of aggregates from the present simulations and the measurements of Ref. [8]. The boxes capture the lower quartile, median (black line) and upper quartile values. The blue line that extended from the box shows the upper and the lower fence. The red dots show the average length of the aggregations in each case. Plots for particle concentrations: a) 0.563 mg/ml, b) 1.125 mg/ml, c) 2.25 mg/ml, and d) 4.5 mg/ml. (For interpretation of the references to colour in this figure legend, the reader is referred to the web version of this article.)

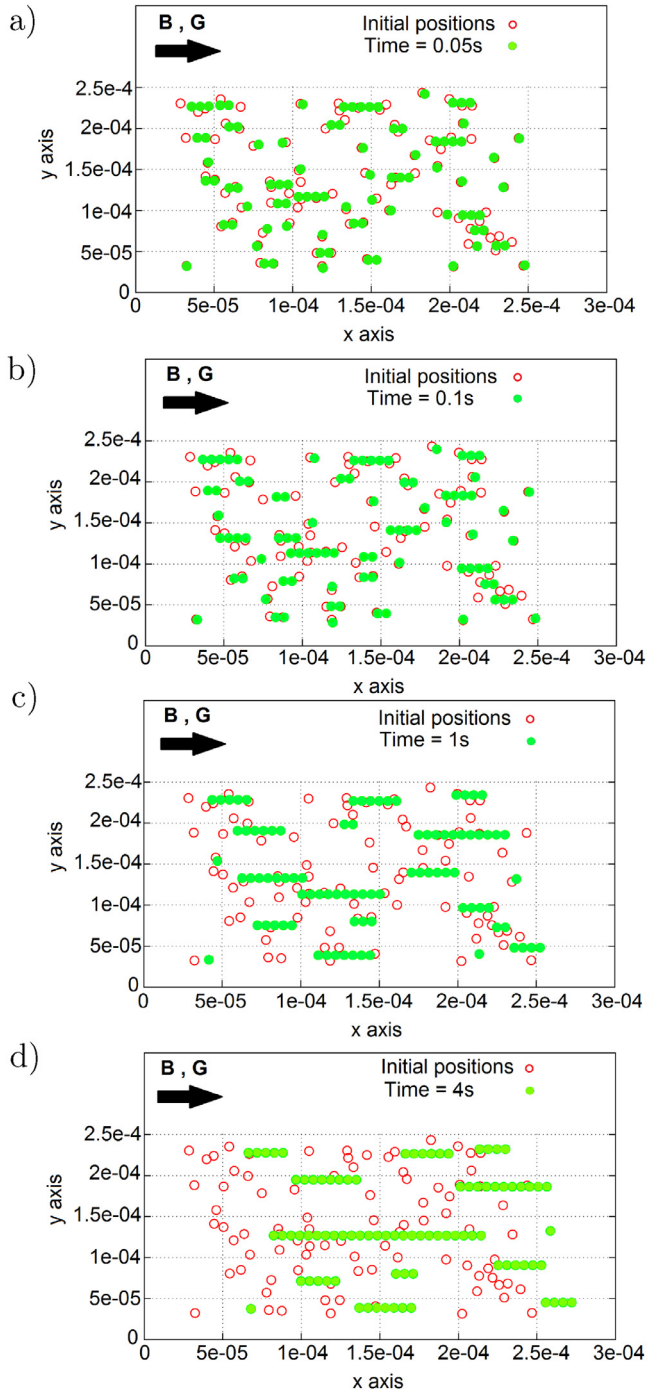

Fig. 3. Starting positions of particles (red circles) and final positions (green filled circles) for particles displacement between $t = 0$ s and: a) $t = 0.05$ s, b) $t = 0.1$ s, c) $t = 1$ s, and d) $t = 4$ s. (For interpretation of the references to colour in this figure legend, the reader is referred to the web version of this article.)

of B_0, higher values of $\bar{l}_a$ are observed for the bigger particles of 22 μm due to the attraction of greater amounts of bigger particles, which form the aggregations.

As shown in Fig. 4a for the case of simulations with the 11 μm particles, the mean chain consists on average by 2.22 particles for $B_0 = 0.1T$. On the other hand, in the case with the 22 μm particles and the same B_0, the mean chain consists on average by 4.64 particles. As B_0 increases, the slope of $\bar{l}_a$ for the 22 μm particles is steeper than for the 11 μm one, and for $B_0 = 1T$ the difference in $\bar{l}_a$ is found to be up to 500 μm. This occurs due to the higher magnetic force which is exerted from the particles that is proportional to their volume [41]. The values of $\bar{l}_a$ for the two series of simulations is found to fit according to the relation: $\bar{l}_a = 7.5 B_0 d_i^{3/2}$ as shown in Fig. 4b.

The variation of some major axis length quantities of the aggregations as B_0 increases is shown in Fig. 5. Apart the mean length

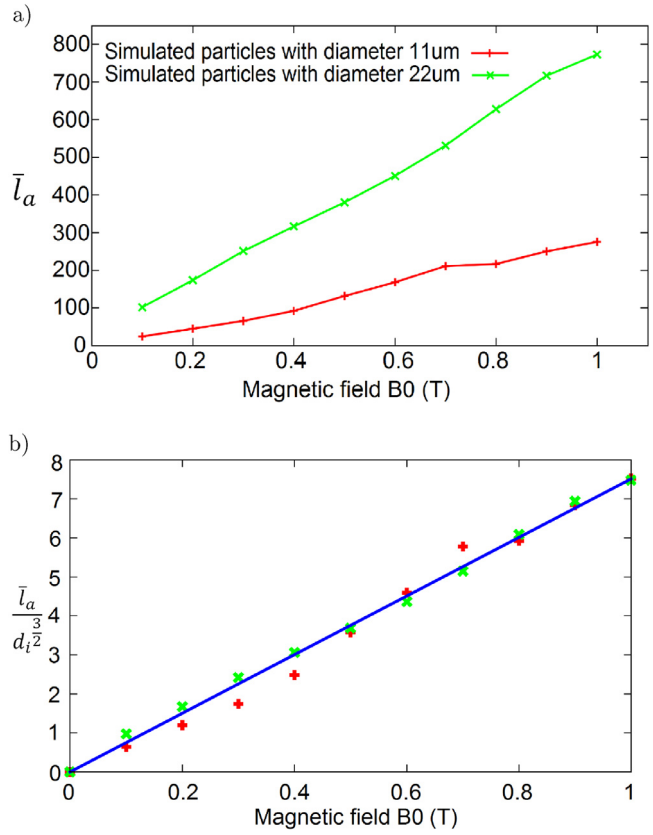

Fig. 4. Mean length of aggregations, $\bar{l}_a$, for various B_0: a) for particles with diameter 11 μm (Red line, + symbols) and 22 μm (Green line, × symbols), and b) values and the data fit relationship: $\bar{l}_a = 7.5B_0\ d_i^{3/2}$, with both $\bar{l}_a$ and d_i in μm. (For interpretation of the references to colour in this figure legend, the reader is referred to the web version of this article.)

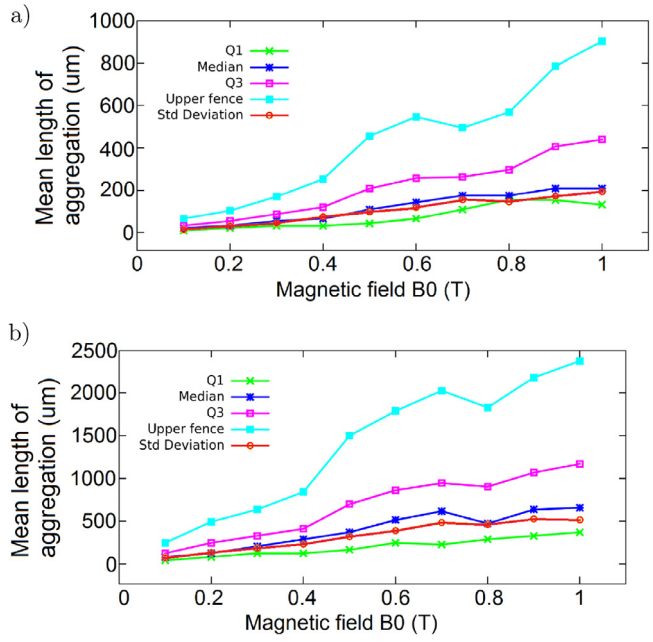

Fig. 5. Distribution of several length quantities of the aggregations for various B_0 for particles with diameter: a) $d_1 = 11$ μm, and b) $d_2 = 22$ μm.

Table 5
Mean length and number of particles in aggregations for various B_0.

Magnetic field $B_0(T)$	Mean length of aggregation in μm		Mean number of particles in aggregation	
	$d_i = 11$ μm	$d_i = 22$ μm	$d_i = 11$ μm	$d_i = 22$ μm
0.1	24.46	102.13	2.22	4.64
0.2	44.71	173.66	4.06	7.89
0.3	65.73	250.94	5.97	11.40
0.4	92.28	316.43	8.38	14.38
0.5	131.73	456.25	11.97	20.73
0.6	168.09	575.81	15.28	26.17
0.7	211.19	624.91	19.19	28.40
0.8	216.79	627.61	19.71	28.52
0.9	250.38	716.61	22.76	32.57
1	275.57	772.90	25.05	35.13

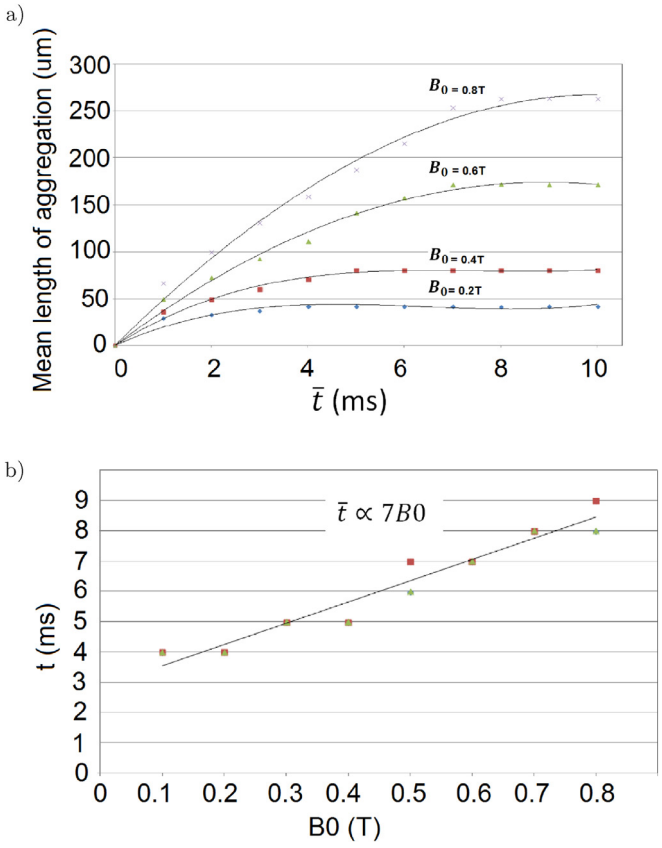

Fig. 6. Time evolution for the formation of aggregations for various B_0 : a) the mean length of aggregations during simulations, b) the total times needed for the aggregations to form. The line $\bar{t}_a \propto 7B_0$ is plotted after least square fitting of the data.

and standard deviation of the chain sizes, the upper values of the chains length can also be read. Moreover, the quantities Q_1 and Q_3 in the same plot represent the upper and the lower quartile values of the lengths of the chains, respectively. As it is depicted in Fig. 5, the magnitude of the magnetic field, for both kinds of particles with 11 μm and 22 μm diameter, can influence strongly the mean length of aggregations and their standard deviation. Thus, it is found that, the mean length of aggregations is more uniform for the low magnitudes of B_0 and as the magnetic field increases the size of aggregations is widely spread. Similarly, it is also observed that uniformity is higher in aggregations consisted of small particles than those of the larger diameter.

The time evolution of the mean length of aggregations for the 11 μm particles is shown in Fig. 6a for various B_0. It is observed that stable length of aggregations is formed sooner for the lower

values of B_0 than for the higher one. This is coherent with the size, i.e. the mean length of aggregations in the case of small B_0 because chains are shorter due to the reduced magnetic force and interaction distance [36]. On the other hand, $\bar{l}_a$ is getting longer for the higher values of B_0, and, more time is required for the elongated chains to completely form in this case. The average time needed by the aggregations to be formed, $\bar{t}_a$, for various B_0 is shown in Fig. 6b, for both the 11 μm and 22 μm particles. As B_0 increases, $\bar{t}_a$ is found to increase almost linear. The least square fitting of $\bar{t}_a$ for the B_0 range is scaled according to the relationship $\bar{t}_a \propto 7B_0$.

Thus, as B_0 and $\bar{t}_a$ linearly increase the magnetic moment of particles have stronger potential to attract them together and from greater distances to form bigger aggregations, as is depicted in Fig. 7 for $B_0 = 0.1T$, $0.4T$ and $0.7T$. As B_0 is increased from $0.1T$ to $0.7T$, almost no more single particles can be observed in the domain and only the longer aggregations are increased in quantity.

4.2. Effect of gradient magnetic field

As previously, two series of simulations for particles with diameter 11 μm and 22 μm are performed by increasing the gradient magnetic field $\tilde{G}$ between 0 and 1 T/m. On top of $\tilde{G}$, a permanent magnetic field B_0 is also applied in order to force particles to form aggregations. We observe that the application of B_0 is essential for the efficient motion of particles because the constant magnetic field makes particles to attract each other and to form aggregations, while in the absence of B_0, the magnetic moment of single particles is so weak that is difficult for $\tilde{G}$ to move them. As aggregations are formed by the attraction magnetic force due to B_0, particles are accelerated after a critical length is achieved by the magnetic gradient in the parallel to $\tilde{G}$ direction, as it is reported also in Ref. [42], until a constant velocity is succeed upon time.

The use of $\tilde{G}$ in the magnetic microparticle applications is primarily to drive them inside the flow stream and not to influence the aggregation process. The present model is used to verify this property of $\tilde{G}$ and to investigate the possible effect of $\tilde{G}$ to influence the mean length of aggregations and the total time needed by the particles to form the aggregations. The mean length of aggregates for various $\tilde{G}$ is shown in Fig. 8 for $B_0 = 0.5T$ and $1T$ where not a great variance in $\bar{l}_a$ is observed. An almost similar result is also extracted for the effect of $\tilde{G}$ at the total time $\bar{t}_a$ to form the mean aggregations (not shown here). Thus, it is observed only B_0 can influence $\bar{l}_a$ and $\bar{t}_a$ during the aggregation formation and magnetic driving of the particles, and $\tilde{G}$ can basically affect the motion of particles, as is also observed by Kim et al. [43].

The dependance of mean velocity of the aggregates, $\bar{u}_a$, for various gradient magnetic fields is showed in Fig. 9a. As $\tilde{G}$ increases, the velocity of particles is increased proportional for both kinds of particles. This increase is rather linear for the range of $\tilde{G}$ used in the present simulations. Apart from $\tilde{G}$, d_i also influences $\bar{u}_a$. The aggregates of particles with the bigger diameter are observed to move with higher $\bar{u}_a$ than the aggregates of the smaller particles due to their larger magnetic volume. However, particles diameter is very weak to influences very weakly $\bar{u}_a$, i.e. no more than a few percentage points although d_i increases 100%. In contrast, B_0 is found to influence $\bar{u}_a$ in a similar degree as $\tilde{G}$. For the 11 μm particles for example, as $\tilde{G}$ is doubled from 0.5 to 1 T/m, $\bar{u}_a$ is more than doubled, in the same time, when B_0 is increased from 0.5 to $1T$, $\bar{u}_a$ is also increased by up to 100%. Thus, in the range of $\tilde{G}$ and B_0 used here, both types of magnetic fields are found to be important for the driving of particles. The linear dependance of $\bar{u}_a$ from both $\tilde{G}$ and B_0 is shown in Fig. 9b in the least-square fitted line of the results: $\bar{u}_a = 6.63\tilde{G}B_0$.

The mean velocity of the aggregates needs more than $2s$ to be fully developed as is shown in Fig. 10 for the indicative case of $B_0 = 1T$, $\tilde{G} = 1$ T/m and $d_i = 22$ μm. This time is significantly larger than $\bar{t}_a$ because of the slow acceleration of the aggregates by $\tilde{G}$ due to the fluid environment. After this time, the mean velocity of aggregates is found to remain asymptotically constant. It should be also noticed however that $\bar{u}_a$ measures the mean velocity of the aggregates that may be different than the local velocity of a single chain. After $\bar{t}_a$, large and small aggregates or even sin-

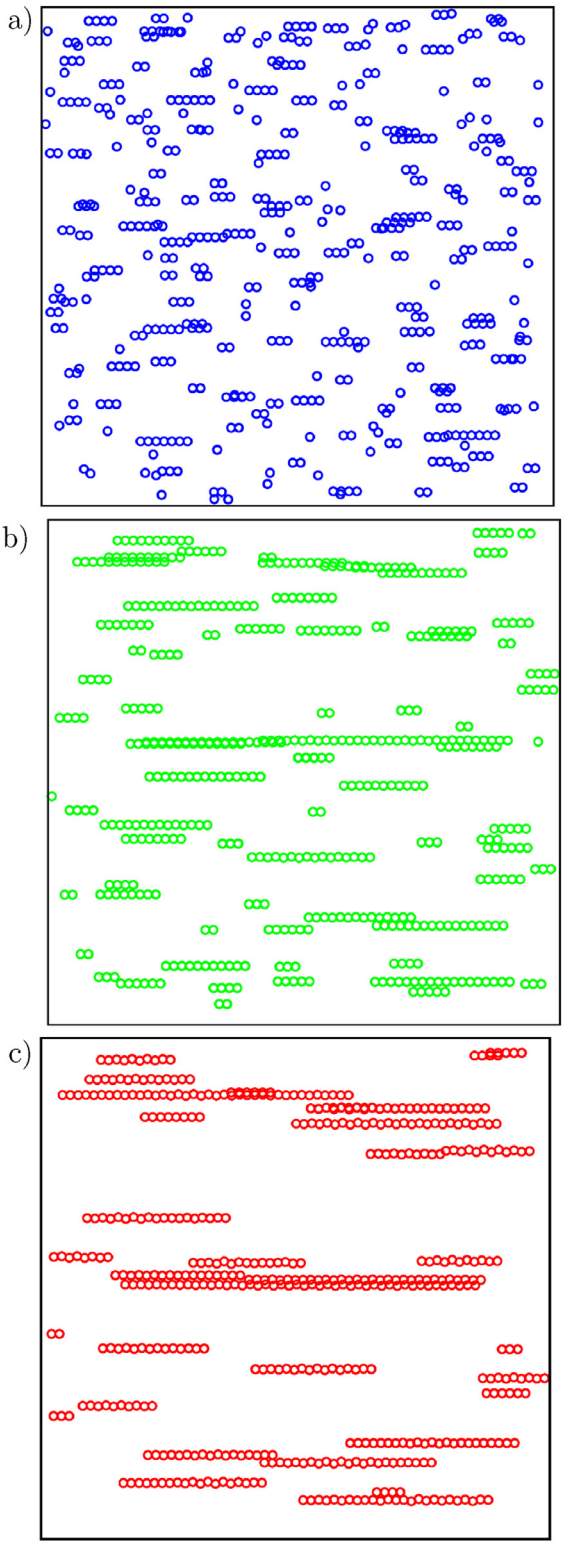

Fig. 7. 2D projections of the formed aggregations under steady magnetic fields of magnitude: a) $0.1T$, b) $0.4T$, and c) $0.7T$.

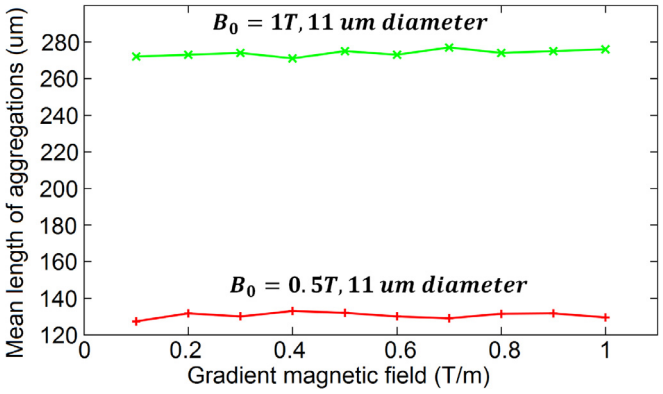

Fig. 8. Mean length of aggregations for various $\tilde{G}$ and $B_0 = 0.5T$ and $1T$, for particles with diameter of 11 μm.

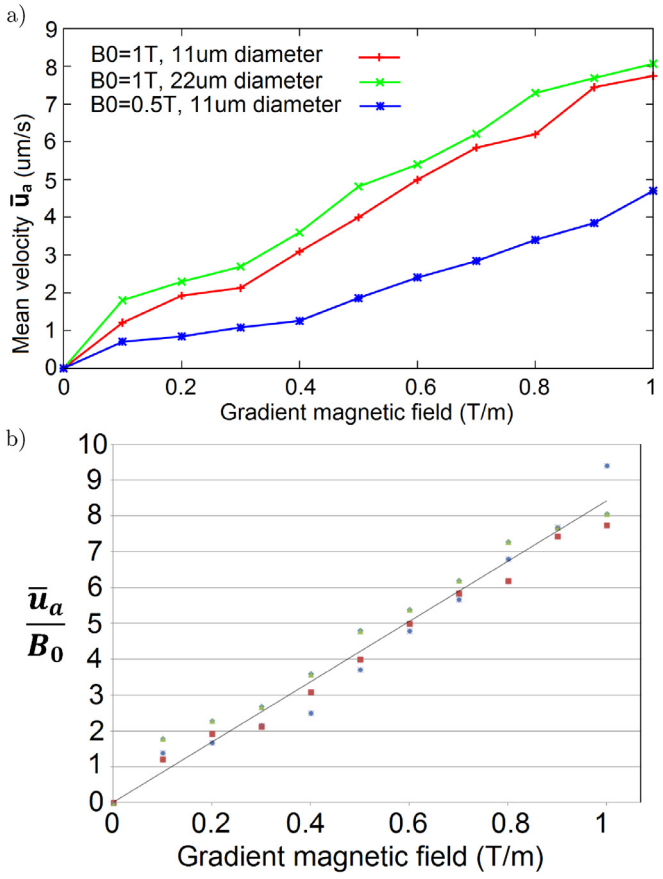

Fig. 9. Mean velocity of aggregations for various $\tilde{G}$ for the two kinds of particles and $B_0 = 0.5T$ and $1T$: (a), measured quantities of u_a, and b) the data-fit line $\bar{u}_a = 6.63\tilde{G}B_0$. u_a in μm/s.

gle particles are moving due to $\tilde{G}$ with different magnetic forces and thus different velocities [43]. The large aggregates are magnetically accelerated faster than the small ones. These aggregates except of attracting single particles that are moving with lower velocity can also attract parallel chains, although this is a near field effect [44]. These events are showed in Fig. 10 for one small and one large chain, that are monitored during their motion. The size of the large aggregate is increased by 38 particles and the size of the small aggregate by 6 particles.

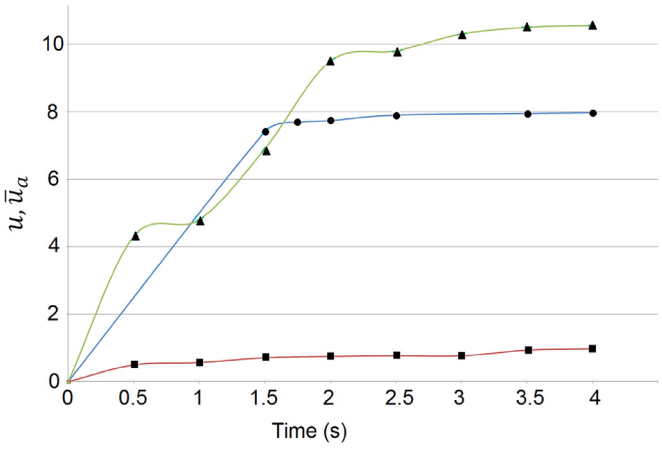

Fig. 10. Mean velocity $\bar{u}_a$ of aggregates (blue line with '•'), velocity u of a single chain for the case $B_0 = 1T$, $\tilde{G} = 1$ T/m and $d_i = 22$ μm. Green line with '▲' corresponds to the velocity of a large monitoring chain ($\bar{l}_a = 27d_i$) and red line with '■' corresponds to the velocity of a small monitoring ($\bar{l}_a = 3d_i$) chain where gaps indicate acceleration when single particles or smaller aggregates merge. (For interpretation of the references to colour in this figure legend, the reader is referred to the web version of this article.)

5. Conclusions

Although magnetic targeting has been successful in a number of studies, there remains only a small number of clinical trials to date, since there are problems and boundaries that further investigation in needed [45,46].

A numerical model to predict the motion of magnetic particles for medical applications is developed. The present model is used to investigate the effect of the permanent magnetic field magnitude B_0, the magnetic gradient $\tilde{G}$ and the diameter of spherical particles d_i in the aggregation and in the driving process inside the flow. This model is found suitable to predict the formation of aggregations and their motion under the action of permanent and gradient magnetic fields, respectively, that are produced by an MRI device. Results of the present model are found to be in good agreement against existing experimental and numerical measurements [8,24].

Moreover, the numerical model is used to measure the mean length of aggregations, the total time needed to form and their mean velocity under different permanent and gradient magnetic fields. The main results are summarized by the following relationships:

$$\text{mean length: } \bar{l}_a = 7.5B_0 d_i^{3/2}$$
$$\text{mean velocity: } \bar{u}_a = 6.63\tilde{G}B_0$$
$$\text{total time: } \bar{t}_a \propto 7B_0$$

Thus, the mean length of aggregations is proportional to the constant magnetic field B_0 and diameter of particles. The mean velocity of the aggregations is equally proportional to the gradient magnetic field $\tilde{G}$ and B_0. Finally, the total time needed for the particles to form the mean aggregations is proportional to B_0. From the above findings, is obvious that the magnitude of the external constant magnetic field is the most important parameter for the aggregations formation and their driving. As B_0 increases, all three quantities, $\bar{l}_a$, $\bar{u}_a$ and $\bar{t}_a$ linearly increase. $\tilde{G}$ is found to be important only in the driving velocity of aggregates and no effect on $\bar{l}_a$ and $\bar{t}_a$ is observed for the range of the used parameters.

Acknowledgements

The work is funded by the NANOTHER program (Magnetic Nanoparticles for targeted MRI Therapy) through the Operational

Program COOPERATION 2011 of GSRT, Greece. Discussions with Dr Klinakis from BRFAA, Greece and Prof. Zergioti from NTUA, Greece are also acknowledged.

References

[1] M.K. Lima-Tenorio, E.A.G. Pineda, N.A. Ahmad, H. Fessi, A. Elaissari, Magnetic nanoparticles: in vivo cancer diagnosis and therapy, Int. J. Pharm. 493 (2015) 313–327.

[2] A. Senyei, K. Widder, C. Czerlinski, Magnetic guidance of drug carrying microspheres, Appl. Phys. 49 (1978) 3578–3583.

[3] K. Widder, A. Senyei, G. Scarpelli, Magnetic microspheres : a model system of site specific drug delivery in vivo, Proc. Soc. Exp. Biol. Med. 158 (1978) 141–146.

[4] Q. Pankhurst, J. Connolly, S. Jones, J. Dobson, Applications of magnetic nanoparticles in biomedicine, J. Phys. D: Appl. Phys. 36 (13) (2003) 167–181.

[5] M. Ramezanpour, S.S.W. Leung, K.H. Delgado-Magnero, B.Y.M. Bashe, J. Thewalt, D.P. Tieleman, Computational and experimental approaches for investigating nanoparticle-based drug delivery systems, Biochim. Biophys. Acta 1858 (2016) 1688–1709.

[6] V.P. Podduturi, I.B. Magana, D.P. O'Neal, P.A. Derosa, Simulation of transport and extravasation of nanoparticles in tumors which exhibit enhanced permeability and retention effect, Comput. Methods Programs Biomed. 112 (2013) 58–68.

[7] J. Llandro, J.J. Palfreyman, A. Ionescu, C.H.W. Barnes, Magnetic biosensor technologies for medical applications: a review, Med. Biol. Eng. Comput. 48 (2010) 977–998.

[8] J.B. Mathieu, S. Martel, Aggregation of magnetic microparticles in the context of targeted therapies actuated by a magnetic resonance imaging system, J. Appl. Phys. 106 (4) (2009) 044904–044907.

[9] P. Babinec, A. Krafcik, M. Babincova, J. Rosenecker, Dynamics of magnetic particles in cylindrical halbach array: implications for magnetic cell separation and drug targeting, Med. Biol. Eng. Comput. 48 (2010) 745–753.

[10] M.A. Correa-Duarte, M. Grzelczak, V. Salgueriniño-Maceira, M. Giersig, L.M. Liz-Marzán, M. Farle, K. Sierazdki, R. Diaz, Alignment of carbon nanotubes under low magnetic fields through attachment of magnetic nanoparticles, J. Phys. Chem. B 109 (41) (2005) 19060–19063.

[11] D.H. Nquyen, J.S. Lee, J.H. Choi, K.M. Park, Y. Lee, K.D. Park, Hierarchical self-assembly of magnetic nanoclusters for theranostics: tunable size, enhanced magnetic resonance imagability, and controlled and targeted drug delivery, Acta Biometerialia 35 (2016) 109–117.

[12] S. Ijaz, S. Nadeem, Examination of nanoparticles as a drug carrier on blood flow through catheterized composite stenosed artery with permeable walls, Comput. Methods Programs Biomed. 133 (2016) 83–94.

[13] S. Nadeem, S. Ijaz, Impulsion of nanoparticles as a drug carrier for the theoretical investigation of stenosed arteries with induced magnetic effects, J. Magn. Magn. Mater. 410 (2016) 230–241.

[14] K. Widder, P. Marino, R. Morris, A. Senyei, Targeted Drugs, Wiley, New York, 1983.

[15] J. Zhou, K. van Netten, K. Galvin, Magnetically driven hydrodynamic interactions of magnetic and non-magnetic particles, Chem. Eng. Sci. 63 (13) (2008) 3431–3437.

[16] K. van Netten, J. Zhou, K. Galvin, R. Moreno-Atanasio, Influence of magnetic and hydrodynamic forces on chain-aggregation and motion of magnetisable particles and composites, Chem. Eng. Sci. 93 (2013) 229–237.

[17] B. Gleich, N. Hellwig, H. Bridell, R. Jurgons, C. Seliger, C. Alexiou, B. Wolf, T. Weyh, Design and evaluation of magnetic fields for nanoparticle drug targeting in cancer, IEEE Trans. Nanotechnol. 6 (2) (2007) 164–169.

[18] T. Kubo, T. Sugita, S. Shimose, Y. Nitta, Y. Ikuta, T. Murakami, Targeted delivery of anticancer drugs with intravenously administered magnetic liposomes in osteosarcoma-bearing hamsters, Int. J. Oncol. 17 (2) (2000) 309–315.

[19] B. Yellen, Z. Forbes, D. Halverson, Targeted drug delivery to magnetic implants for therapeutic applications, Magn. Mater. 293 (2005) 647–654.

[20] A.M. Pavlov, S.A. Gabriel, G.B. Sukhorukov, D.J. Gould, Improved and targeted delivery of bioactive molecules to cells with magnetic layer-by-layer assembled microcapsules, Nanoscale 7 (2015) 9686–9693.

[21] H.G. Weller, G. Tabor, H. Jasak, C. Fureby, A tensorial approach to computational continuum mechanics using object-oriented techniques, Comput. Phys. 12 (6) (2010) 620–631.

[22] L. Waite, Biofluid Mechanics in Cardiovascular Systems, McGraw-Hill's, New York, 2005, pp. 123–126.

[23] A.I. Iatridis, I.E. Sarris, N.S. Vlachos, Transition of an electromagnetically driven liquid metal flow from laminar to turbulent in a toroidal square duct, EPL (Europhysics Letters) 101 (4) (2013) 44005.

[24] P. Vartholomeos, C. Mavroidis, In silico studies of magnetic microparticle aggregations in fluid environments for MRI-guided drug delivery, IEEE Trans. Biomed. Eng. 59 (11) (2012) 3028–3038.

[25] E. Tijskens, H. Ramon, J.D. Baerdemaeker, Discrete element modelling for process simulation in agriculture, J. Sound Vib. 266 (2003) 493–514.

[26] N.K. Lampropoulos, E.G. Karvelas, I.E. Sarris, Computational modeling of an MRI guided drug delivery system based on magnetic nanoparticle aggregations for the navigation of paramagnetic nanocapsules, 11th world congress on computational mechanics, in: 5th European Conference on Computational Mechanics and 6th European Conference on Computational Fluid Dynamics, 2014, pp. 823–847.

[27] H.A. Roque, Structure and Functional Properties of Colloidal Systems, CRC Press, Taylor & Francis Group, London, 2009, pp. 120–131.

[28] S.C. Glotzer, M.J. Solomon, N.A. Kotov, Self-assebly ; from nanoscale to microscale colloids, AIChE 50 (12) (2004) 2978–2985.

[29] M. Oda, K. Iwashita, Mechanics of Granular Materials ; An introduction, CRC Press, Taylor & Francis Group, London, 1999, pp. 355–358.

[30] E. Climent, M.R. Maxey, G.E. Karniadakis, Dynamics of self-assembled chaining in magnetorheological fluids, Langmuir 20 (2004). 507-213.

[31] K.W. Yung, P.B. Landecker, D.D. Villani, An analytic solution for forces between two magnetic dipoles, Magn. Electr. Sep. 9 (1998) 39–52.

[32] J.D. Jackson, Classical Electrodynamics, 3rd ed., Wiley, New Jersey, 1998, pp. 184–190.

[33] C.L. Epstein, F.W. Wehrli, Magnetic resonance imaging, 2005, http://www.math.upenn.edu/~cle/papers/nmri_sngl.pdf, (accessed 17/01/2017).

[34] A. Mehdizadeh, R. Mei, J. Klausner, N. Rahmatian, Interaction forces between soft magnetic particles in uniform and non-uniform magnetic fields, Acta Mechanica Sinica/Lixue Xuebao 26 (6) (2010) 921–929.

[35] T. Fujita, M. Mamiya, Interaction forces between nonmagnetic particels in the magnetized magnetic fluid, J. Magn. Magn. Mater. 65 (1987) 207–210.

[36] N.K. Lampropoulos, E.G. Karvelas, I.E. Sarris, Computational study of the particles interaction distance under the influence of steady magnetic field, J. Adv. Syst. Sci. Appl. 15 (3) (2015) 227–236.

[37] T. Sato, M. Kanke, H.G. Schroeder, P.P. DeLuca, Porous biodegradable microspheres for controlled drug delivery, assessment of processing conditions and solvent removal techniques, Pharm. Res. 5 (1) (1988) 21–30.

[38] Y. Tang, Q.W. Chen, R. Chen, Magnetic field induced controllable self-assembly of maghemite nanocrystals: from 3d arrays to 1D nanochains, Appl. Surf. Sci. 347 (2015) 202–207.

[39] H. Takahashi, D. Nagao, K. Watanabe, H. Ishii, M. Konno, Magnetic field aligned assembly of nonmagnetic composite dumbbells in nanoparticle-based aqueous ferrofluid, Langmuir 31 (2015) 5590–5595.

[40] M. Wang, L. He, Y. Yin, Magnetic field guided colloidal assembly, Mater. Today 16 (4) (2013) 110–116.

[41] J.A. Ruiz-López, J. C.Fernández-Toledano, R. Hidalgo-Alvarez, J. Vicente, Testing the mean magnetization approximation, dimensionless and scaling numbers in magnetorheology, Soft Matter 12 (2016) 1468–1476.

[42] D. Heinrich, A.R.G. ni, T.M. Osán, L.M.C. Cerioni, A. Smessaert, S.H.L. Klapp, J. Faraudo, D.J. Pusiol, C. Thomsen, Effects of magnetic field gradients on the aggregation dynamics of colloidal magnetic nanoparticles, Soft Matter 11 (2015) 7606–7616.

[43] S. Kim, F. Qiu, S. Kim, A. Ghanbari, C. Moon, L. Zhang, B.J. Nelson, H. Choi, Fabrication and characterization of magnetic microrobots for three-dimensional cell culture and targeted transportation, Adv. Mater. 28 (41) (2013) 5863–5868.

[44] R. Messina, I. Stanković, Assembly of magnetic spheres in strong homogeneous magnetic field, Physica A 466 (2017) 10–20.

[45] J. Estelrich, E. Escribano, J. Queralt, M.A. Busquets, Iron oxide nanoparticles for magnetically-guided and magnetically-responsive drug delivery, Int. J. Mol. Sci. 16 (2015) 8070–8101.

[46] B.K. Lee, Y.H. Yun, K. Park, Smart nanoparticles for drug delivery: boundaries and opportunities, Chem. Eng. Sci. 125 (2015) 158–164.